Hardware-in-the-Loop Simulation of Robust Gain-Scheduling Control of Port-Fuel-Injection Processes

Andrew White, *Student Member, IEEE*, Guoming (George) Zhu, and Jongeun Choi, *Member, IEEE*

***Abstract*—In this paper, an event-based sampled discrete-time linear system representing a port-fuel-injection process based on wall-wetting dynamics is obtained and formulated as a linear parameter varying (LPV) system. The system parameters used in the engine fuel system model are engine speed, temperature, and load. These system parameters can be measured in real time through physical or virtual sensors. A gain-scheduling controller for the obtained LPV system is then designed based on the numerically efficient convex optimization or linear matrix inequality (LMI) technique. A hardware-in-the-loop (HIL) simulation is performed to validate the gain-scheduling controller on a mixed mean-value and crank-based engine model. The HIL simulation results show the effectiveness of the proposed gain-scheduling controller.**

***Index Terms*—Engine and powertrain control, gain-scheduling control, hardware-in-the-loop (HIL) simulation, LPV control, robust control.**

I. Introduction

INCREASING concerns about global climate change and ever-increasing demands on fossil fuel capacity call for reduced emissions and improved fuel economy. Vehicles equipped with a port-fuel-injection fuel system have been widely used today; and vehicles equipped with a direct-injection (DI) fuel system have been introduced to markets globally. In order to improve DI engine full load performance at high speed, Toyota introduced an engine with a stoichiometric direct injection system with two fuel injectors for each cylinder (see [1]). One is a DI injector generating a dual-fan-shaped spray with wide dispersion, while the other is an intake port injector. The dual-fuel system introduces one additional degree of freedom for engine optimization to reduce emissions with improved fuel economy. The use of gasoline port-fuel-injection and ethanol DI dual-fuel system to substantially increase gasoline engine efficiency is described by [2]. The main idea is to use a highly boosted small turbocharged engine to match the performance of a much larger engine. Direct injection of ethanol is used to suppress engine knock at high-engine load due to its substantial air charge cooling resulting from its high heat of vaporization. This shows that with the introduction of DI fuel systems for the internal combustion engine, port-fuel-injection fuel systems will be part of the engine fuel system for improved engine performance, which is the main motivation for revisiting the air-to-fuel ratio control problem for a port-fuel-injection fuel system.

There have been several fuel control strategies developed for internal combustion engines to improve the efficiency and exhaust emissions. A key development in the evolution was the introduction of a closed-loop fuel injection control algorithm [3], followed by the linear–quadratic control method [4], and an optimal control and Kalman filtering design [5]. Specific applications of A/F ratio control based on observer measurements in the intake manifold were developed by [6]. Another approach was based on measurements of exhaust gases A/F ratio measured by the oxygen sensor and the mass air flow rate close to the throttle position [7]. A nonlinear sliding mode control of A/F ratio based upon the oxygen sensor feedback was also developed in [8]. Continuing research efforts of A/F ratio control include adaptive approaches [9], [10], observer-based controllers [11], H_∞ controllers [12], model predictive controllers [13], sliding mode controllers [14], and linear parameter-varying controllers [15]–[17]. Conventional A/F ratio control for automobiles uses both closed-loop feedback and feedforward control to have good steady state and fast transient responses.

For a spark-ignited engine equipped with a port-fuel-injection system, the wall-wetting dynamics is commonly used to model the fuel injection process; and the wall-wetting effects are compensated on the basis of simple time-invariant linear models that are tuned and calibrated through engine dynamometer and vehicle tests. These models are quite effective for an engine operated at steady state or slow transition conditions but they are difficult to be used at fast transient and other special operational conditions, for instance, during engine cold start. One of the approaches to model the wall-wetting dynamics during engine cold start is to describe it using a family of linear models to approximate the system dynamics at a given engine coolant temperature, speed and load conditions, that is, to translate the fuel system model into a linear parameter varying (LPV) system.

As stated earlier, the use of LPV modeling to control the A/F ratio of a port-fuel-injection system has been reported by [15]–[17]. In [17], a continuous-time, LPV model is developed considering only engine speed as a time-varying parameter. Due to the simplicity of the model used, the issue of engine cold start is not addressed. Furthermore, the control synthesis method

Manuscript received March 22, 2010; revised August 25, 2010; accepted November 13, 2010. Manuscript received in final form November 19, 2010. Date of publication January 06, 2011; date of current version September 16, 2011. This work was supported in part by the Department of Energy under Grant DE-FC26-07NT43275. Recommended by Associate Editor K. Ropke.

The authors are with the Department of Mechanical Engineering, Michigan State University, East Lansing, MI 48824 USA (e-mail: whitea23@egr.msu.edu; zhug@egr.msu.edu; jchoi@egr.msu.edu).

Color versions of one or more of the figures in this paper are available online at http://ieeexplore.ieee.org.

Digital Object Identifier 10.1109/TCST.2010.2095420

used in [17] relies on gridding the parameter space at a finite number of grid points. In [16], a large variable time delay is present in the air–fuel ratio control loop for a lean burn spark-ignition engine. LPV control methods are used to compensate for the variable time delay. In [15], a discrete-time, LPV model is developed with manifold absolute pressure, exhaust value closing, and inlet value opening as the time-varying parameters. However, only manifold absolute pressure is used as a scheduling parameter in the gain-scheduling control that is synthesized. Also, [15] does not address the issue of engine cold start. Additionally, all LPV control synthesis methods used by [15] are based in continuous time, relying on Tustin's (bilinear) transformation to convert the discrete-time system to a continuous-time system, thus fixing the engine speed and sampling rate of the discrete-time system. In contrast to all of these efforts, this paper designs an event-based gain-scheduling controller for an event-based discrete-time LPV system with wall-wetting parameters and engine speed as time-varying parameters. To cope with practical situations, the discrete-time LPV control synthesis method given by [18] is used to develop the event-based gain-scheduling controller. An affine LPV model including the feedforward control dynamics is obtained. Gain-Scheduling controllers have been synthesized to guarantee the robust stability and performance of the affine LPV model.

The control structures used in this study are proportional-integral (PI) and proportional-integral-derivative (PID). PI controllers are widely used in industry, since they are well understood by field control engineers. The PI gains are often calibrated in field tests for the best performance as functions of system operational conditions. However, the system stability and performance are not guaranteed for all time-varying parameters. Therefore, LPV techniques proposed in this paper are applied to design gain-scheduling PI controllers for guaranteed stability and performance for all time-varying parameters. Furthermore, the addition of derivative control to a PI controller adds an extra layer of complexity. The design of a PID controller at a single operating point can be a difficult iterative procedure, which would make calibrating PID gains as functions of system operational conditions very time consuming. However, designing a gain-scheduling PID controller using LPV techniques is as simple as adding a derivative channel to the control input. The ability to design either a gain-scheduling PI or PID controller with guaranteed stability and performance in one shot without requiring hours of calibration will be well received by industrial control engineers.

The process of designing an LPV controller for any automotive application is shown in Fig. 1. Due to the complexity of internal combustion engines, designing controllers for specific engine systems using an entire engine model is extremely difficult if even possible. Therefore, to design a controller for a specific engine subsystem, first a physics-based simplified model is developed to represent the engine subsystem. After the varying parameters are identified, the physics-based model can be transformed into an LPV model. LPV controller design can then be carried out on the LPV model to develop an LPV controller. Once the LPV controller is obtained it must be tested on the original engine to ensure that it meets all stability and performance requirements. A cost effective way of validating developed LPV controllers is to implement them in a rapid prototyping real-time control systems and validate them through HIL simulations.

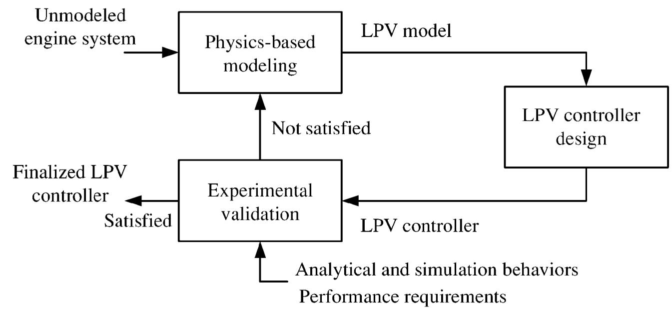

Fig. 1. Flowchart of the design and validation process of an LPV controller.

In this paper, we first develop a physics-based model for the port-fuel-injection process based on the wall-wetting dynamics and formulate it as an LPV system. The system parameters used in the engine fuel system model are engine speed, temperature, and load. These system parameters can be obtained in real time through physical or virtual sensors. A gain-scheduling controller is then obtained for the derived LPV system based on the numerically efficient convex optimization (or LMI) techniques. To validate the gain-scheduling PI and PID controllers, HIL simulations were performed using a mixed mean-value and crank-based engine model [19].

Standard notation is used throughout the paper. Let $\mathbb{R}$ and $\mathbb{Z}_{\geq 0}$ denote the set of real and non-negative integer numbers, respectively. The positive definiteness of a matrix A is denoted by $A > 0$. The maximum (respectively, minimum) of α is denoted by $\overline{\alpha}$ (respectively, $\underline{\alpha}$). Other notation will be explained in due course.

II. LPV Gain-Scheduling Controller Design

The design of the LPV gain-scheduling controller is explained in full detail by [20].

A. Plant Dynamics

1) Dynamics of Port-Fuel-Injection Process: The discrete-time linear system is obtained by event-based sampling of the port-fuel-injection process, hence the sampling time of this discrete-time system is the period of an engine cycle (see general engine modeling techniques in [21]). The wall-wetting dynamics can be described as follows:

$$\begin{aligned} m_w(k) &= (1-\beta_k)m_i(k) + (1-\alpha_k)m_w(k-1) \\ m_c(k) &= \beta_k m_i(k) + \alpha_k m_w(k-1) \end{aligned} \tag{1}$$

where $k \in \mathbb{Z}_{\geq 0}$, and m_i, m_w, and m_c denote the amounts of fuel, injected, on the wall and in the cylinder, respectively. The coefficients $\alpha \in [0,1]$ and $\beta \in [0,1]$ are the ratios of the fuel delivered from the wall to the cylinder, and of the fuel entering the cylinder from injection, respectively.

The wall wetting parameters (α and β) of a port-fuel-injection process are typically identified at different engine speeds, loads, and temperatures during a so-called engine mapping process with an engine dynamometer, and then 3-D surfaces are created for the wall wetting parameters (α and β) as functions of engine

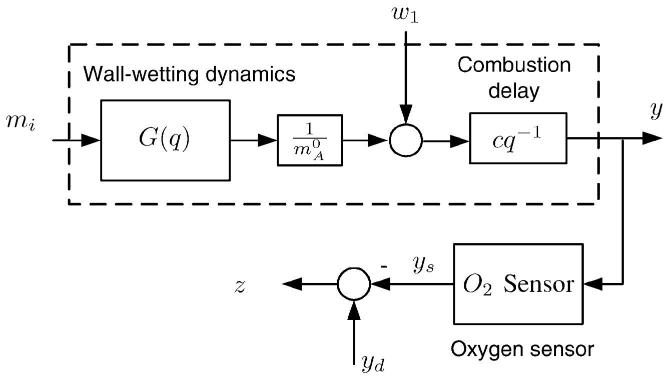

Fig. 2. Block diagram of the port-fuel-injection process and sensor dynamics.

speed, load, and temperature. These three LPV parameters, engine speed, load, and temperature, represent the leading variations of the wall wetting dynamics. The wall wetting dynamics can also be obtained through adaptive estimation [22]. Using the either of these techniques, the wall wetting parameters α and β can be estimated online, which allows us to apply gain-scheduling control to the plant. Using the discrete-time dynamics in (1), we obtain the transfer function $G(q)$ from m_i to m_c

$$G(q) := \frac{m_c(k)}{m_i(k)} = \frac{\beta_k + (\alpha_k - \beta_k)q^{-1}}{1-(1-\alpha_k)q^{-1}} \tag{2}$$

where q is the *forward shift operator* that satisfies

$$qu(k) = u(k+1).$$

The dotted box in the block diagram in Fig. 2 illustrates the fuel-injection process. The output of $G(q)$ is the input to the gain block of $(1)/(m_A^0)$, which is the nominal value of the inverse of the air amount m_A. The signal w_1 represents the deviation $((m_c)/(m_A)-(m_c)/(m_A^0))$ [14], which will be treated as a disturbance in this paper. Another constant gain factor $c = 14.6$ in Fig. 2 is the value for the air-to-fuel ratio at stoichiometric. After the combustion delay block the equivalence ratio y (inverse of the normalized air-to-fuel ratio) is generated. The diagram of the transfer function from the amount of fuel injected m_i and the disturbance w_1 to the equivalence ratio y is shown in the dotted box in Fig. 2.

2) Oxygen Sensor: To measure y, we use an oxygen sensor whose dynamics are modeled as the first-order dynamics; and the transport delay of the exhaust gas mixture is modeled as a function of engine speed $T_D = (80/N)$ where N denotes the speed of the engine in revolutions per minute (r/min). The combined transfer function in the continuous time domain is

$$y_s(s) = \frac{\exp(-T_D s)}{T_{O_2}s+1} y(s) \tag{3}$$

where y_s is the equivalence ratio measured by the sensor and T_{O_2} is the time constant of the oxygen sensor. Since the delay $T_D \in [(80/\bar{N}), (80/\underline{N})]$ is small, (3) can be approximated by the second-order system

$$y_s(s) = \frac{1}{T_D s+1}\frac{1}{T_{O_2}s+1} y(s)$$

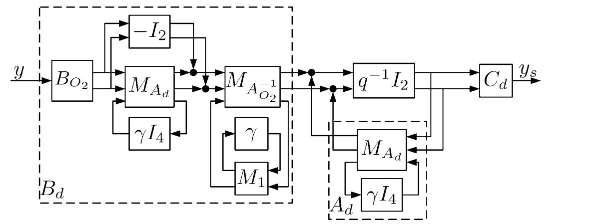

Fig. 3. Block diagram of the combined dynamics of the exhaust gas and sensor delays.

that has the state-space representation

$$\begin{bmatrix} \dot{x}_1 \\ \dot{x}_2 \end{bmatrix} = \underbrace{\begin{bmatrix} -\frac{1}{T_D} & \frac{1}{T_D} \\ 0 & -\frac{1}{T_{O_2}} \end{bmatrix}}_{=:A_{O_2}} \begin{bmatrix} x_1 \\ x_2 \end{bmatrix} + \underbrace{\begin{bmatrix} 0 \\ \frac{1}{T_{O_2}} \end{bmatrix}}_{=:B_{O_2}} y$$
$$y_s = \underbrace{\begin{bmatrix} 1 & 0 \end{bmatrix}}_{=:C_{O_2}} x. \tag{4}$$

The event-based controller updates the control every combustion event such that the sample period is given by $t_s = (120/N)$. Using t_s as the sampling period, the corresponding discrete system of (4) is

$$\begin{aligned} x(k+1) &= A_d x(k) + B_d y(k) \\ y_s(k) &= C_d x(k) \end{aligned}$$

where

$$\begin{aligned} A_d &= \exp(A_{O_2} t_s) \\ B_d &= \left(\int_0^{t_s} \exp(A_{O_2}\tau) d\tau\right) B_{O_2} = A_{O_2}^{-1}(A_d - I)B_{O_2} \\ C_d &= C_{O_2}. \end{aligned}$$

Since both T_D and t_s are functions of engine speed N, naturally A_d and B_d are as well. A fourth-order Taylor series approximation is used to capture the parameter variation of A_d. To ensure that the coefficients of the Taylor series approximation of A_d are numerically stable, the engine speed N must be normalized. Furthermore, due to the way that N appears in $A_{O_2}^{-1}$, it is necessary to isolate $(1/N)$ instead of N. For this reason, we normalize $(1/N) \in [(1/\bar{N}), (1/\underline{N})]$ to γ in the following way:

$$\gamma = \frac{\frac{1}{N} - \frac{1}{N_0}}{\frac{1}{N} + \frac{1}{N_0}} \quad \text{where} \quad \frac{1}{N_0} = \frac{\frac{1}{\bar{N}} + \frac{1}{\underline{N}}}{2}. \tag{5}$$

The polynomial linear fractional transformations M_{A_d} and $M_{A_{O_2}^{-1}}$, given in [20], are used to isolate the varying parameter [23]. The diagram of the transfer function from the equivalence ratio y to the measured equivalence ratio y_s is shown in Fig. 3.

B. Control Synthesis

The objective of the control system is to regulate the equivalence ratio y to a reference input y_d using feedback control against the disturbance signal w_1. To achieve the objective, a unified control design scheme is proposed in which a gain-scheduling feedback controller $K(\Theta)$ is designed for the feedforward control compensated generalized plant P (see

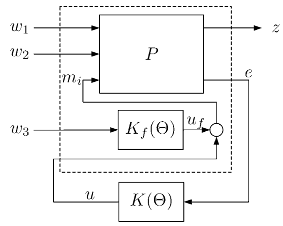

Fig. 4. Proposed control strategy for the fuel injection process. The LPV control strategy is applied to the systems inside the dotted box. Here $w_2 = y_d$ and $w_3 = m_A\, y_d$.

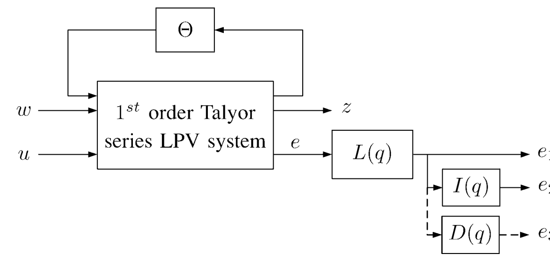

Fig. 5. First-order Taylor series LPV system augmented with the low-pass filter $L(q)$, integrator $I(q)$, and differentiator $D(q)$ (only for PID controller).

[20]), as depicted in Fig. 4. The feedforward controller $K_f(\Theta)$ is designed using the inverse of $cG(q)$

$$K_f(\Theta) = \frac{G^{-1}(q)}{c} = \frac{1}{c}\left(\frac{1-(1-\alpha_k)q^{-1}}{\beta_k + (\alpha_k - \beta_k)q^{-1}}\right).$$

The systems inside the dotted box in Fig. 4 are formulated as a discrete-time LPV system using linear fractional transformation (LFT). Then the gain-scheduling controller $K(\Theta)$ is designed based on the technique given by [18].

In the generalized plant P, the time-varying parameters α_k and β_k are considered to be equivalent to a constant nominal value plus a time-varying fluctuation. For instance, the parameter variation of $\alpha_k \in [\underline{\alpha}, \bar{\alpha}]$ with $\alpha_0 = ((\underline{\alpha} + \bar{\alpha})/(2))$ would be represented by

$$\alpha_\delta(k) = \alpha_k - \alpha_0 \in [\underline{\alpha} - \alpha_0, \bar{\alpha} - \alpha_0]$$

so that the parameter range of α_δ is centered around zero. Hence, α_k is replaced by $\alpha_0 + \alpha_\delta(k)$. The same is done for $\beta_k \in [\underline{\beta}, \bar{\beta}]$ as well.

With the parameter variation represented in this way, the system is written as a discrete-time LPV system with LFT parameter dependency,

$$\begin{bmatrix} l(k) \\ x(k+1) \\ z(k) \\ e(k) \end{bmatrix} = \underbrace{\left[\begin{array}{c|ccc} D_{00} & C_0 & D_{01} & D_{02} \\ \hline B_0 & A & B_1 & B_2 \\ D_{10} & C_1 & D_{11} & D_{12} \\ D_{20} & C_2 & D_{21} & D_{22} \end{array}\right]}_{=:M} \begin{bmatrix} p(k) \\ x(k) \\ w(k) \\ u(k) \end{bmatrix}$$
$$p(k) = \Theta(k) l(k). \tag{6}$$

where $x(k) \in \mathbb{R}^n$ is the state at time k, $w(k) \in \mathbb{R}^r$ is the disturbance, $z(k) \in \mathbb{R}^p$ is the error output, $p(k), l(k) \in \mathbb{R}^{n_p}$ are the pseudo-input and output connected by $\Theta(k)$, $u(k) \in \mathbb{R}^m$ is the control input, and $e(k) \in \mathbb{R}^q$ is the measurement for control. The time-varying parameter Θ in (6) follows the structure:

$$\Theta \in \boldsymbol{\Theta} = \{\mathrm{diag}(\beta_\delta I_3, \alpha_\delta I_2, \gamma I_9) : |\alpha_\delta| \le \delta_1, |\beta_\delta| \le \delta_2, |\gamma| \le 1\} \tag{7}$$

where $\delta_1 = (\bar{\alpha} - \underline{\alpha}/2)$ and $\delta_2 = (\bar{\beta} - \underline{\beta}/2)$.

The ℓ_2 gain of the LPV system in (6) with a gain-scheduling feedback controller is defined as

$$\max_{\Theta \in \boldsymbol{\Theta}, \|w\|_2 \neq 0} \frac{\|z\|_2}{\|w\|_2}. \tag{8}$$

Problem: The goal is to design a static gain-scheduling control $u(k) = K(\Theta)e(k)$ that minimizes the ℓ_2 gain of the closed-loop LPV system in (8).

By inspection of the LPV system in (6), D_{00} was found to be a nonzero block. Hence, the system matrices are not affine functions of parameters. To utilize the control synthesis technique given by [18], the first-order Taylor series approximation of the system matrices is used to obtain affine functions in Θ. Notice that (6) is an upper LFT, i.e.,

$$H(\Theta) := \mathcal{F}_u(M, \Theta). \tag{9}$$

Using the Taylor series expansion at $\Theta = 0$, the system can be approximated as

$$\hat{H}(\Theta) = H(0) + \beta_\delta[\nabla H(0)]_1 + \alpha_\delta[\nabla H(0)]_2 + \gamma[\nabla H(0)]_3$$

where $[\nabla H(0)]_i$ is the partial derivative of the LFT system $H(\Theta)$ in (9) with respect to the ith parameter, which can be calculated as shown by [24].

The control synthesis technique given by [18] also requires that the output matrix $\hat{C}_2$ be independent of the time-varying parameters and the output e must not be corrupted by the disturbance input $w(k)$ ($D_{21} = 0$ in (10)). To accomplish this, the error output e is filtered with a low-pass filter (see Fig. 5)

$$L(q) = \frac{0.9999}{q - 0.0001405}.$$

Integral action was introduced to eliminate steady-state error for the step input y_d

$$I(q) := \frac{e_2(k)}{e_1(k)} = \frac{1}{q-1}.$$

Derivative action is introduced, when designing a PID controller, to enhance the response of the closed-loop system when large changes in w_1 are present [25]

$$D(q) := \frac{e_3(k)}{e_1(k)} = \frac{F(q-1)}{(F+1)q - 1}.$$

F is chosen to set the location of the pole of the derivative filter. Notice that $I(q)$ and $D(q)$ are not functions of the sampling period t_s. This is due to the requirement that, as previously stated, the output matrix $\hat{C}_2$ be independent of the time-varying parameters. For this reason, $I(q)$ is really just a numerical summation and $D(q)$ is a filtered numerical differencer.

The first-order Taylor series LPV system is augmented with $L(q), I(q)$, and $D(q)$ (if designing a PID controller) as shown in Fig. 5 to recover the discrete-time polytopic linear time-varying system

$$\begin{bmatrix} x(k+1) \\ z(k) \\ \hat{e}(k) \end{bmatrix} = \begin{bmatrix} \hat{A}_{[\chi(k)]} & \hat{B}_{1[\chi(k)]} & \hat{B}_{2[\chi(k)]} \\ \hat{C}_{1[\chi(k)]} & \hat{D}_{11[\chi(k)]} & \hat{D}_{12[\chi(k)]} \\ \hat{C}_2 & 0 & 0 \end{bmatrix} \begin{bmatrix} x(k) \\ w(k) \\ u(k) \end{bmatrix} \quad (10)$$

where, for all $k \in \mathbb{Z}_{\geq 0}$, $\chi(k)$ is the vector of time-varying parameter weights that belong to the unit simplex

$$\Lambda_{N_v} = \left\{ \zeta \in \mathbb{R}^{N_v} : \sum_{i=1}^{N_v} \zeta_i = 1, \zeta_i \geq 0, i = 1, \ldots, N_v \right\}.$$

A way to compute the weight vector $\chi(k)$ for a given $\alpha_\delta(k)$, $\beta_\delta(k)$, and $\gamma(k)$ is provided by [26]. For all $k \in \mathbb{Z}_{\geq 0}$, the rate of variation of the weights

$$\Delta\chi_i(k) = \chi_i(k+1) - \chi_i(k), \quad i = 1, \ldots, N_v$$

is limited by the calculated bound b such that

$$-b\chi_i(k) \leq \Delta\chi_i(k) \leq b(1 - \chi_i(k)), \quad i = 1, \ldots, N_v \quad (11)$$

where $b \in [0, 1]$.

The system matrices $\hat{A}_{[\chi(k)]} \in \mathbb{R}^{n\times n}$, $\hat{B}_{1[\chi(k)]} \in \mathbb{R}^{n\times r}$, $\hat{B}_{2[\chi(k)]} \in \mathbb{R}^{n\times m}$, $\hat{C}_{1[\chi(k)]} \in \mathbb{R}^{p\times n}$, $\hat{D}_{11[\chi(k)]} \in \mathbb{R}^{p\times r}, and$ $\hat{D}_{12[\chi(k)]} \in \mathbb{R}^{p\times m}$ belong to the polytope

$$\begin{aligned} \mathcal{D} = \{ & (\hat{A}, \hat{B}_1, \hat{B}_2, \hat{C}_1, \hat{D}_{11}, \hat{D}_{12})(\chi(k)) : \\ & (\hat{A}, \hat{B}_1, \hat{B}_2, \hat{C}_1, \hat{D}_{11}, \hat{D}_{12})(\chi(k)) \\ & = \sum_{i=1}^{N_v} \chi_i(k)(\hat{A}, \hat{B}_1, \hat{B}_2, \hat{C}_1, \hat{D}_{11}, \hat{D}_{12})_i, \chi(k) \in \Lambda_{N_v} \}. \end{aligned}$$

A finite set of LMIs in [18] can be used to design the gain-scheduling controller. Due to Theorem 3 of [18], if there exists matrices $G_{i,1} \in \mathbb{R}^{q\times q}$, $G_{i,2} \in \mathbb{R}^{(n-q)\times q}$, $G_{i,3} \in \mathbb{R}^{(n-q)\times(n-q)}$, $Z_{i,1} \in \mathbb{R}^{m\times q}$ and symmetric matrices $P_i \in \mathbb{R}^{n\times n}$ such that the LMI conditions in [18] are satisfied, the gain-scheduling static feedback control is then obtained as

$$K(\chi(k)) = \hat{Z}(\chi(k))\hat{G}(\chi(k))^{-1} \quad (12)$$

where

$$\hat{Z}(\chi(k)) = \sum_{i=1}^{N_v} \chi_i(k) Z_{i,1}$$

and

$$\hat{G}(\chi(k)) = \sum_{i=1}^{N_v} \chi_i(k) G_{i,1}.$$

This control is proved to stabilize affine parameter-dependent systems such as (10) with a guaranteed $\mathcal{H}_\infty$ performance bounded by u for all $\chi \in \Lambda_{N_v}$ and $\Delta\chi$ that satisfies (11).

III. Design of Linear Time-Invariant (LTI) Feedback Controllers

To demonstrate the necessity of a gain-scheduled controller over a LTI controller, we designed a fixed gain $\mathcal{H}_\infty$ controller based on the nominal parameters. Using the nominal parameters, the closed-loop state-space representation is

$$\begin{aligned} x(k+1) &= A_{CL}(K)x(k) + B_1 w(k) \\ z(k) &= C_{CL}(K)x(k) + D_{11} w(k) \end{aligned} \quad (13)$$

where

$$\begin{aligned} A_{CL}(K) &= A + B_2 K C_2 \\ C_{CL}(K) &= C_1 + D_{12} K C_2. \end{aligned}$$

Denoting the transfer function from w to z by H_{wz}, the inequality $\|H_{wz}\|_\infty^2 < \mu$ holds if, and only if, there exists a symmetric matrix P such that

$$\begin{bmatrix} P & A_{CL}(K)P & B_1 & 0 \\ PA_{CL}^T(K) & P & 0 & PC_{CL}^T(K) \\ B_1^T & 0 & I & D_{11}^T \\ 0 & C_{CL}(K)P & D_{11} & \mu I \end{bmatrix} < 0 \quad (14)$$

is feasible [27]. The optimal feedback controller K for the closed-loop system (13) is formulated as the optimization of the bilinear matrix inequality (BMI)

$$\min_{\mu, P, K} \mu \quad \text{subject to (14)} \quad (15)$$

where $P = P^T \in \mathbb{R}^{n\times n}$ and $K \in \mathbb{R}^{1\times 2}$ for a PI controller or $K \in \mathbb{R}^{1\times 3}$ for a PID controller. The BMI (15) was solved using the PENBMI software [28] as a MATLAB function in conjunction with the YALMIP [29] programming interface to find the fixed $\mathcal{H}_\infty$, PID controller $K_{\text{PID}} = [1.4871\ 0.5009\ 0.8942]$.

IV. HIL Simulation Setup

The engine model used for the HIL simulation is a control oriented four cylinder dual fuel mean-value engine model developed at Michigan State University [19], which satisfies the requirements of validating an engine controller. The term "mean-value" indicates that the developed engine model neglects the reciprocating behavior of the engine, assuming all processes and effects are spread out over the engine cycle. For the HIL simulation, this model describes the input-output behavior of the physical engine systems with reasonable simulation accuracy using relatively low computational throughput. Reference [30] provides a good overview of engine modeling, and most of dynamic equations used in our modeling work are from this reference book. This engine model also includes all engine transient dynamics. Fig. 6 shows the overall mean-valve engine model architecture, along with main subsystem models, such

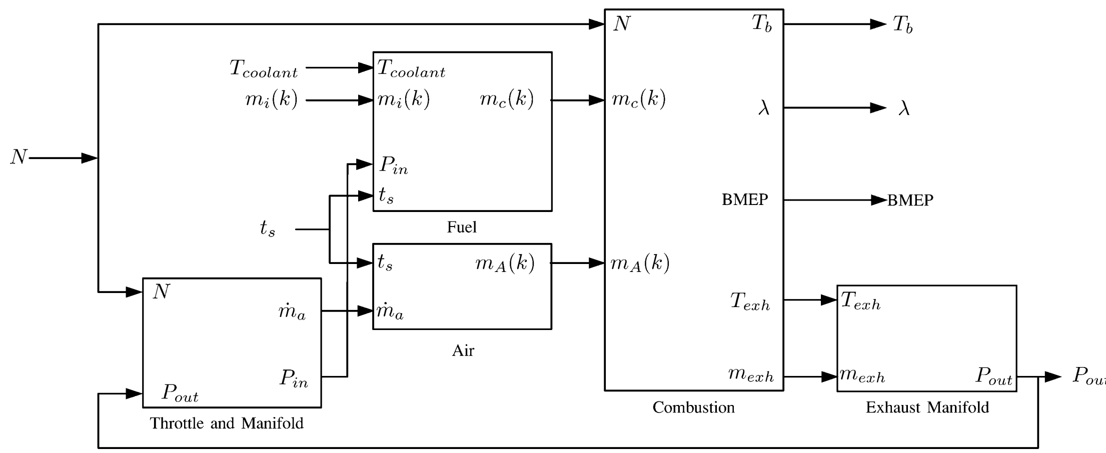

Fig. 6. Mean value engine model.

as air-to-fuel ratio, manifold air pressure, brake mean effective pressure (BMEP), engine torque, exhaust temperature, etc.

A. Mean Value Engine Models

The subsystems that are described mathematically by their averaged dynamic behaviors are given in the following.

1) Valve Model: The valve model is used to compute the mass flow rate of air across the valve. The model used for the intake throttle and the EGR valve follow the governing equations

$$m_v = C_d(\theta)A(\theta)\frac{P_u}{\sqrt{RT_u}}\Psi\left(\frac{P_d}{P_u}\right) \tag{16}$$

and

$$\Psi\left(\frac{P_d}{P_u}\right) = \begin{cases} \sqrt{2\frac{P_d}{P_u}\left(1-\frac{P_d}{P_u}\right)} & \text{if } \frac{1}{2} < \frac{P_d}{P_u} < 1 \\ \frac{1}{\sqrt{2}} & \text{if } \frac{P_d}{P_u} < \frac{1}{2} \end{cases} \tag{17}$$

where C_d is the valve discharge coefficient; θ is the valve opening angle; R is the gas constant; A is the valve open area; P_u and T_u are the pressure and temperature upstream from the valve; and m_v is the mass flow rate across the valve. The governing equations (16)–(17) follow the assumption that the spacial effects of the connecting pipes before and after the valve are neglected and that the thermodynamic characteristics of the connecting pipes are isentropic expansion.

2) Manifold Filling Dynamic Model: The manifold pressure of the intake and the exhaust is computed as a function of time by the governing equation

$$P_m(t) = P_m(0) + \int_0^t \frac{RT_m}{V_m}(m_{\text{in}} - m_{\text{out}})dt \tag{18}$$

where P_m is the manifold pressure; T_m is the manifold temperature; V_m is the manifold volume; m_{in} and m_{out} are the inlet and outlet air mass flow rates; and R is the universal gas constant. The assumptions made by governing equation (18) are that the receiving behavior is an adiabatic process; the thermodynamic states are uniform over the manifold volume; and the manifold temperature is averaged over one engine cycle.

3) Engine Respiration Model: The mass flow rate of the air across of the engine cylinders m_e is computed by the engine respiration model

$$\dot{m}_e = \frac{P_{\text{in}}}{RT_{\text{in}}}\frac{V_d N}{30}\eta\left(\frac{P_{\text{out}}}{P_{\text{in}}}, v\right) \tag{19}$$

where η is a two degree of freedom lookup table; P_{in} and T_{in} are the mean pressure and temperature at the intake manifold; P_{out} is the mean pressure at the exhaust manifold; V_d and V_c are the engine displacement and the cylinder clearance volume; and κ is the heat capacity ratio of the gas charged in the cylinder.

4) Crankshaft Dynamic Model: The crankshaft dynamic model, based on Newton's theory assuming a rigid crankshaft, is derived as

$$\dot{N} = \frac{60}{2\pi}\frac{T_b - T_l}{J_e} \tag{20}$$

where J_e is the rotational inertia of the engine crankshaft; and T_b and T_l are the engine brake and load torques. The desired engine speed is maintained by an engine dynamometer model that generates the engine load torque T_l using a feedback PID controller.

B. Event-Based Engine Models

The mathematical models used to simulate the cycle-to-cycle varying variables of engine subsystems are given in the following. Each variable in this sections is updated based on the engine cycle (k) and is independent of time t.

1) Event-Based Wall-Wetting Dynamics: When port-fuel-injection is used to deliver fuel to the engine cylinders, some of the fuel injected after each injector pulse enters the cylinders. However, the remaining fuel sticks to the walls of the intake port and on the back of the intake valve. The total fuel entering the engine cylinders then consists of fuel injected from the current injection pulse and fuel vapor from the fuel mass stored on the walls from previous injection pulses. Knowledge of this process is necessary to control the metering of fuel for precise air-to-fuel ratio control. The event based wall-wetting dynamics used in the engine for HIL simulation are the same as those in (1).

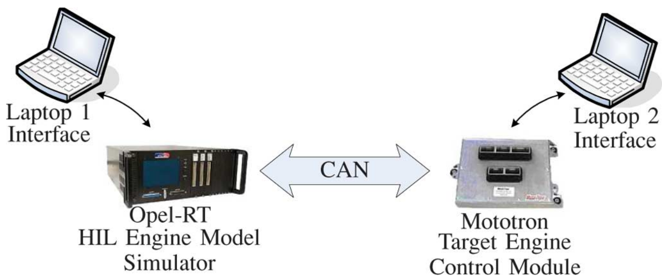

Fig. 7. HIL engine model and controller setup.

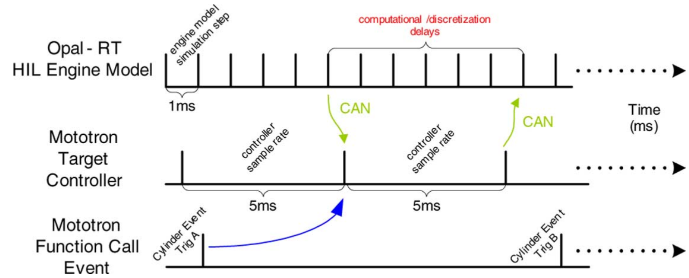

Fig. 8. HIL timing scheme.

2) *Event-Based Engine Air-to-Fuel Ratio:* The gas exchange behavior of the engine introduces dynamics into the air-fuel ratio calculation. Since the engine uses exhaust gas recirculation, a substantial amount of the burned gas remains in the cylinder. The gas fraction carries the air-to-fuel ratio of the previous engine cycle into the current cycle. Due to this behavior, the air-fuel ratio is modeled cycle-to-cycle as

$$\lambda(k) = \frac{\tilde{\lambda}(k)M_{\text{fresh}}(k) + \lambda(k-1)M_{\text{burnt}}(k)}{M_{\text{fresh}}(k) + M_{\text{burnt}}(k)} \tag{21}$$

where $\tilde{\lambda}$ is the normalized air-to-fuel ratio defined as

$$\tilde{\lambda}(k) = \frac{m_A(k)}{m_c(k)}\frac{1}{c}. \tag{22}$$

λ is the normalized air-to-fuel ratio of the gas mixture inside the engine cylinder after the intake valve is closed. M_{fresh} is the mass of the fresh gas mixture charge in the cylinder, which is the summation of the fresh air mass m_A and the fresh fuel mass m_c, and M_{burnt} is the burned gas remaining in the engine cylinder after the exhaust valve closes, which includes burned gas due to both internal and external EGR (exhaust gas recirculation). Note that these dynamics are quite different from the LPV design model described in Fig. 2.

3) *Event-Based Engine Brake Torque:* For every combustion event, the engine brake torque calculation is triggered using the following equation:

$$T_b(k) = \frac{m_c(k)H_l n}{4\pi}\eta_e(N, \lambda, \theta_{\text{st}}, x_{\text{EGR}}) \tag{23}$$

where n is the number of engine cylinders; H_l is the low heating value of the fuel; η_e is the engine efficiency, which is a function of engine speed, normalized air-to-fuel ratio, spark timing θ_{st}, and the exhaust-gas-recirculation rate x_{EGR}.

The mean value engine model was implemented into an Opal-RT HIL system using MATLAB/Simulink. The engine model was updated at a sample period of 1 ms. Similarly, the LPV controller, along with feedforward controller, was implemented as an event-based discrete controller in Simulink into a Mototron engine control module (ECU) sampled every 5 ms as a function call, see HIL simulation scheme shown in Fig. 7. The Opal-RT HIL simulator communicates with the Mototron ECU controller through the high-speed control-area-network (CAN), where signals were sent and received with minimal delay.

The Opal-RT simulation step size of 1 ms was chosen in order to emulate a real-world continuous time engine. Similarly, the Mototron sample rate of 5 ms for the controller updating is used

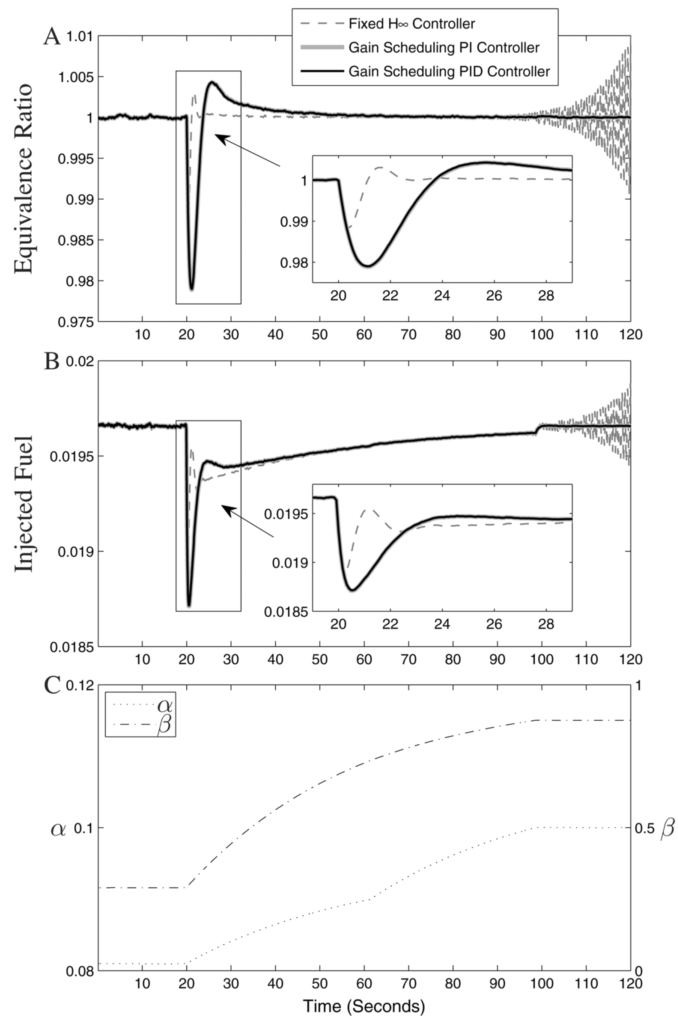

Fig. 9. Case 1: Engine cold start using simple model.

in many production engine control systems. The CAN communication between Opal-RT and Mototron has a time delay between the time when signals are sent from Mototron and the time when they are received by Opal-RT, and vice versa. This delay was less than 1 ms for our setup, since only a few variables were communicated between the HIL simulator and Mototron controller, see the timing scheme in Fig. 8. The event based function call was implemented as follows. At each sample time, the controller checks if the event based sample condition is met; and if so, the function call will be made to execute the event based control strategy (see Fig. 8). Since the sample period of the event-based LPV controller is a function of engine speed

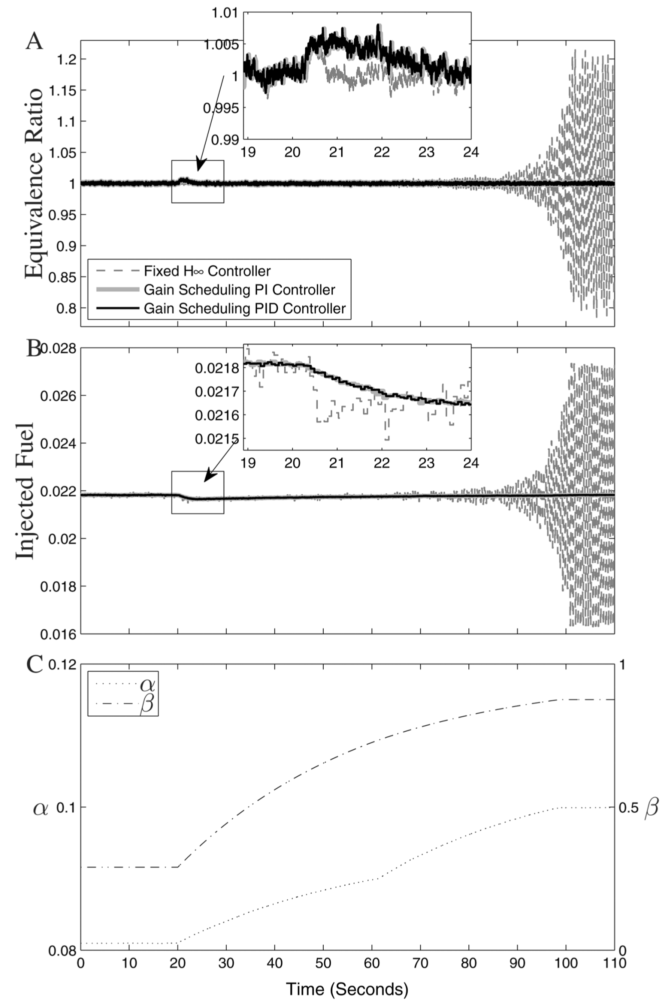

Fig. 10. Case 1: Engine cold start using HIL.

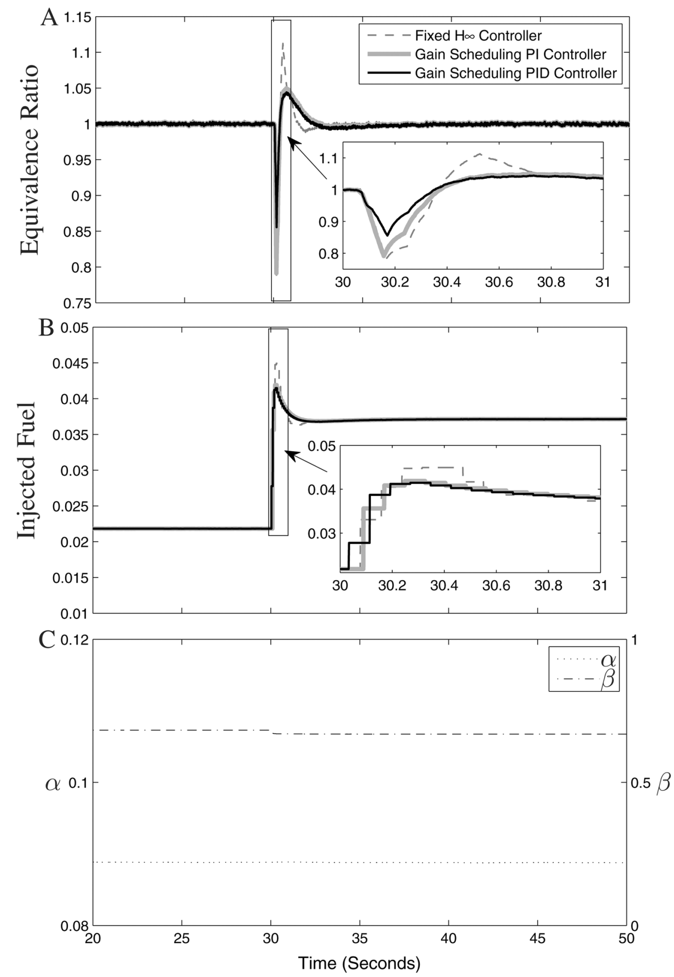

Fig. 11. Case 2: Engine load change using HIL.

and it can executed within a 5 ms sample period, the LPV controller can not be updated exactly at each fuel injection event. This leads to some sample time error between ideal event-based sampling and actual function call implementation.

V. HIL Simulation Results

In Figs. 9–12, the responses for the gain-scheduling PI and PID controllers are given by the solid gray and black lines, respectively. The gray dashed line shows the response of the fixed gain $\mathcal{H}_\infty$ PID controller. In each of the HIL simulations, white Gaussian noise was added to each of the measured signals to represent measurement noise. The standard deviation of the noise added to each signal was set such that the value of the noise would not be larger than the following percentages of the measured signals: air flow $m_A \sim 3\%$, equivalence ratio $y_s \sim 2\%$, coolant temperature $\sim 5\%$, intake pressure $\sim 5\%$, and engine speed $N \sim 1\%$. Even though the cycle-to-cycle combustion variations typically present in internal combustion engines are correlated to engine speed, load and temperatures, the sensor measurement noise, due to cycle-to-cycle combustion variations and sensor noise, was simplified as a Gaussian white noise due to its simplicity and broad bandwidth. Also, in each of the HIL simulations, the fuel injected is saturated, as a function of the mass air flow, to $\pm 25\%$ of the fueling that keeps equivalence ratio at one.

A. Case 1: Engine Cold Start

We simulate an engine cold start process from freezing temperatures (0 °C) to its normal operation temperature of approximately 100 °C within about 2 min at an engine speed of 1500 r/min. The purpose of this simulation is to emulate the cold start of an internal combustion engine when the engine is operated at high idle speed during the warm-up. Note that during the engine warm-up process the fuel vapor is much less at low temperature than that at high temperature. Therefore, this leads to quite different wall-wetting dynamics. The wall-wetting dynamics coefficients α and β defined in (2) were obtained from actual engine test data and they are functions of engine coolant temperature, speed, and load. Since speed and load were fixed in this simulation, both α and β were functions of engine temperature and their values are shown in Fig. 10(C). The responses of the gain scheduling PI and PID controllers during this simulation, given in Fig. 10, are nearly identical. However, at between 100 and 110 s, the fixed gain $\mathcal{H}_\infty$ PID controller becomes saturated causing the measured equivalence ratio to oscillate between 0.8 and 1.2, while both LPV controllers continue to regulate the equivalence ratio to the desired value of 1. Also, in Fig. 10(B), the mass of the fuel injected when using the fixed gain $\mathcal{H}_\infty$ PID controller has noticeable perturbations due to the noise added to the measured equivalence ratio. However, the gain scheduling PI and PID controllers have no noticeable perturbations that demonstrate that not only do they remain stable over the entire operating range of the engine, but also they are robust to the added measurement noise.

For comparison purposes, a simulation was carried out using the control model described in Section II-A for the engine cold start problem with the response displayed in Fig. 9. In this simulation, no measurement noise was added to the measured signals. Also, a saturation level was not imposed on the feedback control input.

B. Case 2: Load Change

In this case we simulate an engine dynamometer experiment for an engine operated at a temperature of 80°C with an engine speed of 1500 r/min. After the engine is stably operated at this condition with a 32% throttle, the load is increased by a step throttle position from 32% to 46%. Note that in the dynamometer test, the engine speed was maintained by dynamometer through torque regulation. This is similar to the driving condition that a step throttle is applied to maintain the vehicle speed when the vehicle is driven up a hill. Note that the step increment of throttle position produces a slight change in the wall-wetting parameter β as shown in Fig. 11(C). The responses of each controller is given in Fig. 11(A). Notice that the throttle step occurring at the 30th second results in a drop in the equivalence ratio due to the step air mass flow. In the detail of Fig. 11(A), we see that with the gain-scheduling PID controller the equivalence ratio only drops to approximately 0.85, while the gain-scheduling PI and fixed gain $\mathcal{H}_\infty$ controller both drop to nearly 0.8. Also, notice that the equivalence ratio with fixed gain $\mathcal{H}_\infty$ PID controller overshot to over 1.1 with over fueling as seen in the detail of Fig. 11(B).

C. Case 3: Engine Speed Change

In this simulation, an engine was operated on a dynamometer with its coolant temperature at 80 °C. To demonstrate the capability for the gain scheduling controller to handle engine speed variations, a smoothed step command from 1500 to 2500 r/min was applied to the engine dynamometer to manipulate the engine speed as shown in Fig. 12(D). The resulting engine wall-wetting dynamics parameters, shown in Fig. 12(C), were used in the simulation. Notice in Fig. 12(A) that the gain-scheduling PID controller regulates the equivalence ratio of the engine to the target value of 1 within 5% error, while the measured equivalence ratio of the engine with the gain-scheduling PI controller and the fixed gain $\mathcal{H}_\infty$ PID controller go above 1.05. Also, the equivalence ratio with the fixed gain $\mathcal{H}_\infty$ PID controller drops to below 0.95, while both gain-scheduling controllers only lower the equivalence ratio to about 0.96. The equivalence ratio with the fixed gain $\mathcal{H}_\infty$ PID controller also has many oscillations and uses more control effort as shown in the detail of Fig. 12(B), which hurts engine transient fuel economy.

D. Case 4: Combined Load and Engine Speed Change

In this simulation, an engine was operated on a dynamometer with its coolant temperature at 80 °C. To demonstrate the capability for the gain scheduling controller to handle load changes combined with engine speed variations, the load is increased by a step throttle position from 32% to 46% and then combined with an engine speed variation generated by a smoothed step command from 1500 to 2000 r/min as shown in Fig. 13(D). The resulting engine wall-wetting dynamics parameters are shown in Fig. 13(C). Notice in Fig. 13(A) both of the gain-scheduling controllers drop the measured equivalence ratio to approximately 0.85, while the fixed gain $\mathcal{H}_\infty$ PID controller drops the measured equivalence ratio below 0.85. Also, the fixed gain $\mathcal{H}_\infty$ PID controller overshoots to nearly 1.15 with over fueling as seen in the detail of Fig. 11(B).

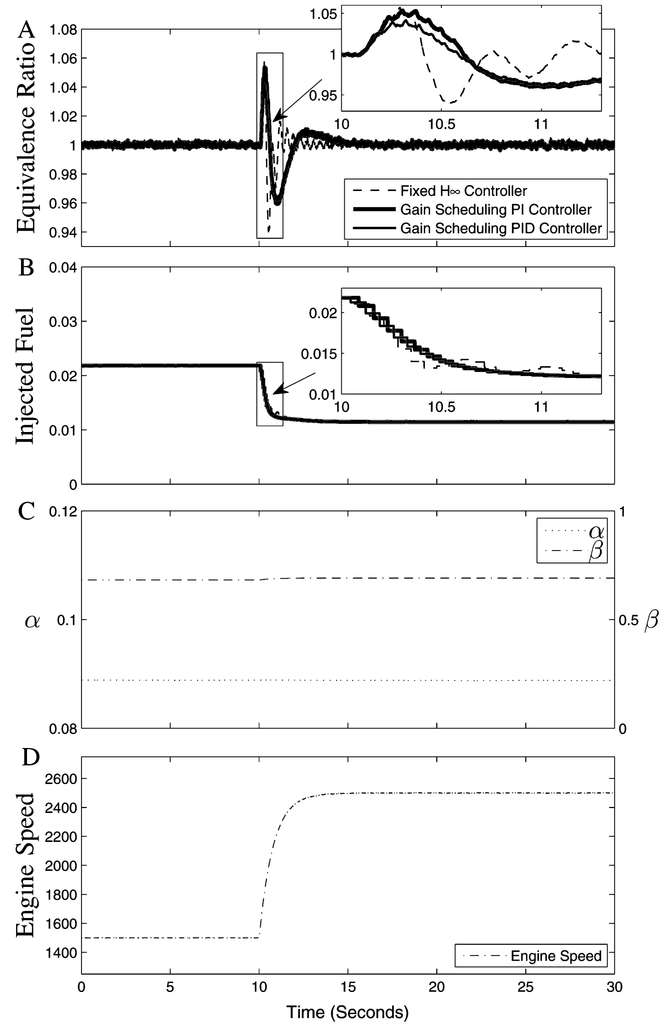

Fig. 12. Case 3: Engine speed change using HIL.

VI. Conclusion

In this paper, an event-based sampled discrete-time linear system representing a port-fuel-injection process based on wall-wetting dynamics was obtained. The system was then formulated as an LPV system with engine speed, temperature, and load as the system parameters in the engine fuel system model. A gain-scheduling controller for the obtained LPV system integrated with the feedforward control dynamics was then designed based on the numerically efficient convex optimization (or LMI) technique. The hardware-in-the-loop simulation results demon-

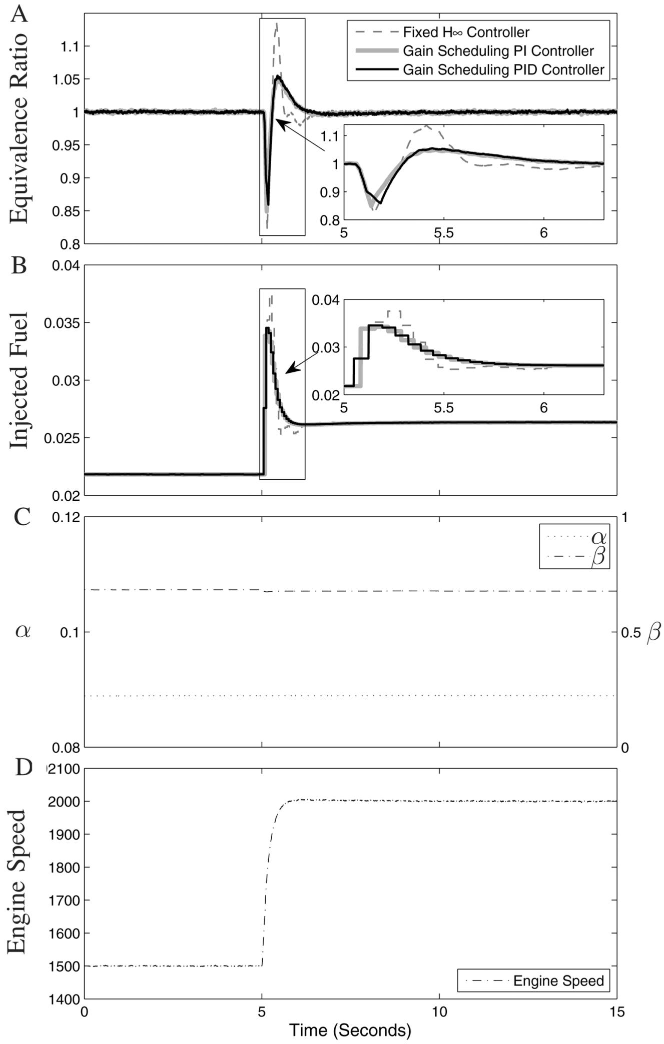

Fig. 13. Case 4: Combined load and engine speed change using HIL.

strate the improvement of the closed-loop system performance over the fixed gain $\mathcal{H}_\infty$ PID controller and the feasibility of implementing of the proposed LPV scheme.

Acknowledgment

The authors would like to thank X. Yang of Michigan State University for providing the mixed mean-value and crank-based engine model used in the HIL simulations.

References

[1] T. Ikoma, S. Abe, Y. Sonoda, H. Suzuki, Y. Suzuki, and M. Basaki, "Development of V-6 3.5-liter engine adopting new direct injection system," SAE, Warrendale, PA, DOI: 10.4271/2006-01-1254, 2006.

[2] J. Heywood, D. Cohn, and L. Bromberg, "Optimized fuel management system for direct injection ethanol enhancement of gasoline engines," U.S. Patent 7 225 787, Jun. 5, 2007.

[3] J. Rivard, "Closed-loop electronic fuel injection control of the internal-combustion engine," SAE, Warrendale, PA, DOI: 10.4271/730005, 1973.

[4] J. Cassidy,, Jr., and M. Athans, "On the design of electronic automotive engine controls using linear quadratic control theory," *IEEE Trans. Autom. Control*, vol. 25, no. 5, pp. 901–912, Oct. 1980.

[5] W. Powers, B. Powell, and G. Lawson, "Applications of optimal control and Kalman filtering to automotive systems," *Int. J. Veh. Des., Special Publication SP4*, pp. 39–53, 1983.

[6] N. Benninger and G. Plapp, "Requirements and performance of engine management systems under transient conditions," SAE, Warrendale, PA, DOI: 10.4271/910083, 1991.

[7] C. Onder, "Model-based multivariable speed and air-to-fuel ratio control of an SI engine," SAE, Warrendale, PA, DOI: 10.4271/930859, 1993.

[8] S. Choi, J. Hedrick, V. Kelsey-Hayes, and M. Livonia, "An observer-based controller design method for improving air/fuel characteristics of spark ignition engines," *IEEE Trans. Control Syst. Technol.*, vol. 6, no. 3, pp. 325–334, May 1998.

[9] R. C. Turin and H. P. Geering, "Model-reference adaptive A/F ratio control in an SI engine based on Kalman-filtering techniques," in *Proc. Amer. Control Conf.*, 1996, pp. 4082–4090.

[10] Y. Yildiz, A. Annaswamy, D. Yanakiev, and I. Kolmanovsky, "Adaptive air fuel ratio control for internal combustion engines," in *Proc. Amer. Control Conf.*, 2008, pp. 2058–2063.

[11] J. Powell, N. Fekete, and C. Chang, "Observer-based air–fuel ratio control," *IEEE Control Syst. Mag.*, vol. 18, no. 5, pp. 72–83, Oct. 1998.

[12] L. Mianzo, H. Peng, and I. Haskara, "Transient air–fuel ratio H_∞ preview control of a drive-by-wire internal combustion engine," in *Proc. Amer. Control Conf.*, 2001, pp. 2867–2871.

[13] K. R. Muske and J. C. P. Jones, "A model-based SI engine air fuel ratio controller," in *Proc. Amer. Control Conf.*, 2006, pp. 3284–3289.

[14] S. Pace and G. G. Zhu, "Sliding mode control of a dual-fuel system internal combustion engine," presented at the in *Proc. ASME Dyn. Syst. Control Conf.*, Hollywood, CA, Oct. 2009.

[15] A. U. Genç, "Linear parameter-varying modelling and robust control of variable cam timing engines," Ph.D. dissertation, Univ. Cambridge, Cambridge, U.K., 2002.

[16] F. Zhang, K. M. Grigoriadis, M. A. Franchek, and I. H. Makki, "Linear parameter-varying lean burn air--fuel ratio control for a spark ignition engine," *J. Dyn. Syst., Meas. Control*, vol. 192, pp. 404–414, 2007.

[17] R. A. Zope, J. Mohammadpour, K. M. Grigoriadis, and M. Franchek, "Air--fuel ratio control of spark ignition engines with TWC using LPV techniques," in *Proc. ASME Dyn. Syst. Control Conf.*, 2009, pp. 897–903.

[18] J. Caigny, J. Camino, R. Oliveira, P. Peres, and J. Swevers, "Gain scheduled H_∞-control of discrete-time polytopic time-varying systems," in *Proc. Conf. Decis. Control*, 2008, pp. 3872–3877.

[19] X. Yang and G. G. Zhu, "A mixed mean-value and crank-based model of a dual-stage turbocharged SI engine for hardware-in-the-loop simulation," in *Proc. 2010 Amer. Control Conf.*, Baltimore, MD, Jun. , pp. 3791–3796.

[20] A. White, J. Choi, R. Nagamune, and G. Zhu, "Gain-scheduling of a fuel injection process," in *Proc. Control Eng. Pract.*, DOI: 10.1016/j.conengprac.2010.12.007.

[21] A. Balluchi, L. Benvenuti, M. D. di Benedetto, C. Pinello, A. L. Sangiovanni-Vincentelli, and R. Parades, "Automotive engine control and hybrid systems: Challenges and opportunities," *Proc. IEEE*, vol. 88, no. 7, pp. 888–912, Jul. 2000.

[22] I. Arsie, C. Pianese, G. Rizzo, and V. Cioffi, "An adaptive estimator of fuel film dynamics in the intake port of a spark ignition engine," *Control Eng. Pract.*, vol. 11, pp. 303–309, 2003.

[23] K. Zhou, J. C. Doyle, and K. Glover, *Robust and Optimal Control*. Englewood Cliffs, NJ: Prentice-Hall, 1996, Upper Saddle River.

[24] R. Nagamune and J. Choi, "Parameter reduction of estimated model sets for robust control," *J. Dyn. Syst., Meas., Control*, vol. 132, no. 2, pp. 021002-1–021002-10, Mar. 2010, DOI: 10.1115/1.4000661.

[25] K. Astrom and B. Wittenmark, *Computer-Controlled Systems: Theory and Design*. New York: Prentice-Hall, 1996.

[26] J. Warren, S. Schaefer, A. N. Hirani, and M. Desbrun, "Barycentric coordinates for convex sets," *Adv. Comput. Math.*, vol. 27, no. 3, pp. 319–338, 2007.

[27] M. C. De Oliveira, J. C. Geromel, and J. Bernussou, "Extended H_2 and H_∞ norm characterizations and controller parametrizations for discretetime systems," *Int. J. Control*, vol. 75, no. 9, pp. 666–679, 2002.

[28] M. Kočcvara and M. Stingl (2006)., PENBMI User's Guide (Version 2.1) 2006 [Online]. Available: http://www.penopt.com, [Online]. Available: http://www.penopt.com

[29] J. Lfberg, "Yalmip: A toolbox for modeling and optimization in MATLAB," in *Proc. Comput.-Aided Control Syst. Des. (CACSD) Conf.*, Taipei, Taiwan, 2004 [Online]. Available: http://control.ee.ethz.ch/~joloef/yalmip.php, [Online]. Available: http://control.ee.ethz.

[30] L. Guzzella and C. H. Onder, *Introduction to Modeling and Control of Internal Combustion Engine Systems*. New York: Springer-Verlag, 2004.

Andrew White (S'10) received the B.S. and M.S. degrees in mechanical engineering from Michigan State University, East Lansing, in 2006 and 2008, respectively. He is currently working toward the Ph.D. degree in the Department of Mechanical Engineering, Michigan State University.

His research interests include adaptive and robust control, and parameter estimation, with applications to engine control, robotics, and nondestructive testing and evaluation.

Guoming (George) Zhu received the B.S. and M.S. degrees from Beijing University of Aeronautics and Astronautics, Beijing, China, in 1982 and 1984, respectively, and the Ph.D. degree in aerospace engineering from Purdue University, West Lafayette, IN, in 1992.

He is an Associate Professor in the Department of Mechanical Engineering (ME), Michigan State University, East Lansing. Prior to joining the ME Department, he was a Technical Fellow in advanced powertrain systems at Visteon Corporation. He also worked for Cummins Engine Co., Ltd. His teaching interests focus on control classes at both undergraduate and graduate levels; and his current research interests include closed-loop combustion control of internal combustion (IC) engines, engine system modeling and identification, hybrid powertrain control and optimization, etc. He has more than 24 years of experience related to control theory, engine diagnostics, and combustion control. He has authored or coauthored more than 100 refereed technical papers and received 39 U.S. patents.

Dr. Zhu is an Associate Editor for the *ASME Journal of Dynamic Systems, Measurement, and Control*.

Jongeun Choi (S'05–M'06) received the B.S. degree in mechanical design and production engineering from Yonsei University, Seoul, Republic of Korea, in 1998. He also received the M.S. and Ph.D. degrees in mechanical engineering from the University of California at Berkeley, Berkeley, in 2002 and 2006, respectively.

He is currently an Assistant Professor in the Departments of Mechanical Engineering, and Electrical and Computer Engineering at Michigan State University, East Lansing. His research interests include adaptive, distributed, and robust control and statistical learning algorithms, with applications to self-organizing systems, mobile robotic sensors, environmental adaptive sampling, engine control, and biomedical problems.

Dr. Choi is a recipient of the National Science Foundation CAREER Award in 2009. He is a member of the ASME.